This is the Pre-Published Version.

This version of the article has been accepted for publication, after peer review (when applicable) and is subject to Springer Nature's AM terms of use (https://www.springernature.com/gp/open-research/policies/accepted-manuscript-terms), but is not the Version of Record and does not reflect post-acceptance improvements, or any corrections. The Version of Record is available online at: https://doi.org/10.1007/s00603-020-02058-7.

Size effects in a transversely isotropic rock under Brazilian tests: laboratory testing

Kaihui Li[a,b], Yungming Cheng[b,c,*], Zhen-Yu Yin[b], Dongya Han[b], Jingjing Meng[a]

1. First author: Kaihui Li

Email : kaihuili_csu@163.com

ORCID: 0000-0002-4763-8680

a. School of Resources and Safety Engineering, Central South University, Changsha, Hunan 410083, China;

b. Department of Civil and Environmental Engineering, The Hong Kong Polytechnic University, Hong Kong, China;

2. Second author (Corresponding author): Yungming Cheng

Email : natureymc@yahoo.com.hk Tel : 852-61525043, Fax : 852-23346389

b. Department of Civil and Environmental Engineering, The Hong Kong Polytechnic University, Hong Kong, China;

c. School of Civil Engineering, Qingdao University of Technology, Qingdao, Shandong 266033, China;

3. Third author: Zhenyu Yin

Email : zhenyu.yin@polyu.edu.hk

b. Department of Civil and Environmental Engineering, The Hong Kong Polytechnic University, Hong Kong, China;

4. Fourth author: Dongya Han

Email : 16901828r@connect.polyu.hk

b. Department of Civil and Environmental Engineering, The Hong Kong Polytechnic University, Hong Kong, China;

5. Fifth author: Jingjing Meng

Email : mengjing120@126.com

a. School of Resources and Safety Engineering, Central South University, Changsha, Hunan 410083, China.

Declaration: There is not any conflict of interest arising from any part of the works in this paper.

Keywords: Slate, transversely isotropic rock, Brazilian test, tensile strength, size effect, anisotropy.

List of symbols

β Angle between the loading direction and the transversely isotropic plane (°)

σ_x, σ_y, and τ_{xy} Stresses in global coordinate system (MPa)

ε_x, ε_y, and γ_{xy} Strains in global coordinate system

q_{xx}, q_{yy}, and q_{xy} Stress concentration factors

a_{ij} Compliance matrix

E and E' Elastic moduli parallel to and perpendicular to the plane of transverse isotropy, respectively (GPa)

ν and ν' Poisson's ratios parallel to and perpendicular to the plane of transverse isotropy, respectively

G' Shear modulus normal to the transversely isotropic plane (MPa)

$T(\beta)$ Tensile strength of a specimen at β (MPa)

T_m and T_b Tensile strength of rock matrix and weak plane, respectively (MPa)

σ_t Tensile strength (MPa)

d Sample diameter (mm)

k Positive constant

σ_{t50} Tensile strength obtained from a specimen of 50 mm in diameter (MPa)

B and λ Dimensionless material constants

f_t and σ_0 Strength of a specimen with an infinitesimal size (MPa)

f_c Strength of a specimen with an infinite size (MPa)

d_0 Maximum aggregate size (mm)

l Material constant (mm)

d_f Fractal dimension

$V_{\max}$, $V_{\min}$ and V_{mean} Maximum, minimum and average ultrasonic wave velocities, respectively (m/s)

$T_1(d)$ and $T_2(d)$ Tensile strength of a specimen with the diameter of d (MPa)

σ_0 and σ_M Tensile strength when $d \to 0$ and $d \to \infty$, respectively (MPa)

$\bar{\sigma}_0$ Tensile strength when $d \to 0$ (MPa)

$T_1(d,\beta)$ and $T_2(d,\beta)$ Tensile strength of a specimen with d at β (MPa)

T_{b0} and T_{m0} Tensile strength of the weak plane and the rock matrix, respectively, when $d \to 0$ (MPa)

T_{bM} and T_{mM} Tensile strength of the weak plane and the rock matrix, respectively, when $d \to \infty$ (MPa)

d_i Specimen diameter at which the maximum tensile strength reaches (mm)

Abbreviations

VA Velocity anisotropy index (%)

MARE Maximum absolute relative error

AARE Average absolute relative error

SE Standard error

Size effects in a transversely isotropic rock under Brazilian tests: laboratory testing

Kaihui Li[a,b], Yungming Cheng[b,c,*], Zhenyu Yin[b], Dongya Han[b], Jingjing Meng[a]

a *School of Resources and Safety Engineering, Central South University, Changsha, Hunan 410083, China*

b *Department of Civil and Environmental Engineering, The Hong Kong Polytechnic University, Hong Kong, China*

c *School of Civil Engineering, Qingdao University of Technology, Qingdao, Shandong 266033, China*

Abstract

A transversely isotropic rock, slate, was utilized to investigate the size effect and anisotropy on its deformation, tensile strength and failure mechanism. A series of Brazilian tests were conducted on slate samples of six different sizes from 25 to 100 mm in diameter at seven different loading-foliation angles from 0° to 90°. The results indicate that the Young's modulus in the plane of transverse isotropy increases, while the Young's modulus and shear modulus perpendicular to the plane of transverse isotropy decrease with specimen size. The tensile strength of the slate increases with increasing loading-foliation angle, the variation of which is well captured by the Nova-Zaninetti criterion. Furthermore, the tensile strength of the slate increases with specimen size at loading-foliation angles from 0° to 45°, while it increases first and then decreases with specimen size at loading-foliation angles from 60° to 90°. A unified size-effect relation including two equations is proposed and verified against the experimental data on slate. The size-effect relation reveals the relationship among the tensile strength, specimen size and loading-foliation angle for the transversely isotropic rock. Last, the slate samples exhibit an increased brittle failure with specimen size, which is

consistent with the observations in various isotropic rocks. It is also found that the specimen size, loading-foliation angle and loading configuration together control the failure mechanism of transversely isotropic rocks in the Brazilian test.

Keywords: Slate, transversely isotropic rock, Brazilian test, tensile strength, size effect, anisotropy.

1. Introduction

In recent years, the behavior of transversely isotropic rocks, e.g., gneiss, schist, slate, phyllite, shale, mudstone and layered sandstone, has attracted increased attention (Fu et al. 2018; Kundu et al. 2018; Sesetty and Ghassemi 2018; Setiawan and Zimmerman 2018; Xu et al. 2018). In general, anisotropic characteristics originate from the stratification in sedimentary rocks, mineral foliation in metamorphic rocks and discontinuities in rock masses (Cho et al. 2012). The anisotropy is one of the most distinct features that must be considered in this kind of rock and is widely encountered in civil, mining, petroleum, geothermal and geo-environmental engineering (Ma et al. 2018).

The tensile strength plays an important role and is often the most vital role in rock engineering because rocks are usually weaker in tension than in compression or shear (Dan et al. 2013). Moreover, tensile failure greatly influences many rock engineering activities, such as drilling, cutting and blasting of rocks, hydraulic fracturing of a wellbore or a tunnel, exploitation of rock slopes, and excavation of underground structures (Chen and Hsu 2001; Goodman 1989). Hence, for engineering practice, the determination of the tensile strength of rocks is indispensable. Compared to the high requirement for experimentation with direct tensile tests (Liao et al. 1997; Shang et al. 2016) or the high requirement for sample preparation with ring tests (Barla and Innaurato 1973; Chen and Hsu 2001), the Brazilian test

is a more common and easy method for measuring the tensile strength of rock. However, the use of the formula for the Brazilian tensile strength requires the material to be isotropic. To improve the Brazilian test so that it can be useful for determining the tensile strength of transversely isotropic rocks, much work has been done by theoretical, experimental and numerical methods (Aliabadian et al. 2017; Cai and Kaiser 2004; Chen et al. 1998; Claesson and Bohloli 2002; Exadaktylos and Kaklis 2001). Among these, a reasonably accurate equation for the principal tension at the rock disc center based on elastic constants and anisotropic angle was proposed (Claesson and Bohloli 2002), which approximates well to the tensile strength of transversely isotropic rocks.

The pioneering work on the anisotropy of tensile strength for transversely isotropic rocks was performed by Hobbs (1964), who conducted Brazilian tests on laminated siltstone, sandstone and mudstone to measure their tensile strengths. Since then, many studies have been carried out on this issue (Ma et al. 2018). The published results showed that the tensile strength of transversely isotropic rocks greatly depended on the angle (β) between the loading direction and the transversely isotropic plane. Based on Brazilian test results of various transversely isotropic rocks, Vervoort et al. (2014) classified four trends for the variation in the tensile strength with β: (1) trend I for which the tensile strength remains constant; (2) trend II for which the tensile strength increases first and then remains constant; (3) trend III for which the tensile strength increases systematically; and (4) trend IV for which the tensile strength remains constant first and then increases linearly. Recently, a U-shaped distribution exhibited by a slate was added into the classification as trend V (Xu et al. 2018). In addition, three typical failure modes have been observed (Dan et al. 2013; Tavallali and Vervoort 2010; Tavallali and Vervoort 2013): (1) fractures along the transversely isotropic planes in the low β range; (2) fractures across the isotropic planes in the high β range; and (3) mixed fractures along and across the isotropic planes in the intermediate β range. Furthermore, Hu et al.

(2017) revealed the main cause for the three failure modes by means of scanning electron microscopy (SEM). The results indicated that with increasing β, the fracture morphology is changed from an intergranular fracture pattern along the bedding plane to that across the rock matrix, and coupled the intergranular fracture with the transgranular fracture when $\beta = 45°$.

When upscaling the strength and elasticity properties obtained from the laboratory to practical engineering design, the size effect must be taken into consideration (Li et al. 2018). As a key input parameter in engineering applications, the size effect on the tensile strength of transversely isotropic rocks must be understood. Nevertheless, the existing size effect relations are almost all derived from isotropic rock or rock-like materials (Bažant 1984; Bažant 1997; Carpinteri et al. 1995; Hoek and Brown 1980; Masoumi et al. 2015), neglecting the influence of rock anisotropy. Consequently, determination of a suitable relation capturing both the size effect and the anisotropy of the tensile strength of transversely isotropic rocks is urgently needed. For this purpose, Brazilian tests were conducted on slate specimens of six different sizes (25-100 mm) at seven various β (0-90°) in this study. During the test, the load and strain data and fracture conditions were recorded. Furthermore, the size effects on the elastic properties, tensile strength and failure mechanism were investigated in detail.

2. Theoretical background

2.1 Constitutive model of transversely isotropic rocks

As presented in Fig. 1, the disc of a transversely isotropic material under diametral loading (Brazilian test) has a diameter D and a thickness t. The angle between the global (x, y, z) and local (x', y', z') coordinate systems is $\pi/2-\beta$, as shown in Fig. 1. The local system is attached to the transversely isotropic plane, with the x'-axis and y'-axis parallel to and perpendicular to the isotropic plane, respectively, and the z'-axis coinciding with the z-axis. If

the disc is loaded with force *P*, the stresses σ_x, σ_y, and τ_{xy} within the disc can be expressed in the form of stress concentration factors (SCFs) q_{xx}, q_{yy}, and q_{xy} (Amadei 1996):

$$\begin{cases} \sigma_x = \dfrac{P}{\pi D t} q_{xx} \\ \sigma_y = \dfrac{P}{\pi D t} q_{yy} \\ \tau_{xy} = \dfrac{P}{\pi D t} q_{xy} \end{cases} \tag{1}$$

A generalized plane stress formulation was used, and the constitutive law is expressed as follows:

$$\frac{\pi D t}{P} \begin{Bmatrix} \varepsilon_x \\ \varepsilon_y \\ \gamma_{xy} \end{Bmatrix} = \begin{bmatrix} a_{11} & a_{12} & a_{16} \\ a_{12} & a_{22} & a_{26} \\ a_{16} & a_{26} & a_{66} \end{bmatrix} \begin{Bmatrix} q_{xx} \\ q_{yy} \\ q_{xy} \end{Bmatrix} \tag{2}$$

As the medium in the direction parallel to the transversely isotropic plane is postulated to be linearly elastic, homogeneous and continuous, Amadei (2012) proposed the expression of a_{ij} as follows:

$$\begin{aligned} a_{11} &= \frac{\sin^4\beta}{E} + \frac{\cos^4\beta}{E'} + \frac{\sin^2 2\beta}{4}\left(\frac{1}{G'} - \frac{2\nu'}{E'}\right) \\ a_{12} &= \frac{\sin^2 2\beta}{4}\left(\frac{1}{E} + \frac{1}{E'} - \frac{1}{G'}\right) - \frac{\nu'}{E'}(\sin^4\beta + \cos^4\beta) \\ a_{16} &= \sin 2\beta\left[\left(\frac{\cos^2\beta}{E'} - \frac{\sin^2\beta}{E}\right) - \left(\frac{1}{2G'} - \frac{\nu'}{E'}\right)\cos 2\beta\right] \\ a_{22} &= \frac{\sin^4\beta}{E'} + \frac{\cos^4\beta}{E} + \frac{\sin^2 2\beta}{4}\left(\frac{1}{G'} - \frac{2\nu'}{E'}\right) \\ a_{26} &= \sin 2\beta\left[\left(\frac{\sin^2\beta}{E'} - \frac{\cos^2\beta}{E}\right) + \left(\frac{1}{2G'} - \frac{\nu'}{E'}\right)\cos 2\beta\right] \\ a_{66} &= \sin^2 2\beta\left(\frac{1}{E} + \frac{1}{E'} + \frac{2\nu'}{E'}\right) + \frac{\cos^2 2\beta}{G'} \end{aligned} \tag{3}$$

where E and E' represent the elastic moduli parallel to and perpendicular to the plane of transverse isotropy, respectively; ν' and G' are the Poisson's ratio and shear modulus in the direction normal to the transversely isotropic plane, respectively. Note that the parameters a_{ij} in Eq. (3) only depend on E, E', ν' and G' and are independent of ν, which is Poisson's ratio in the plane of transverse isotropy.

2.2 Determination of elastic constants for transversely isotropic rocks

Loureiro-Pinto (1979) first determined the elastic constants of anisotropic rocks by means of Brazilian tests. Later, Pinto's procedure was revised by Amadei (1996), and a more accurate solution was given by Chen et al. (1998), who combined the Brazilian test and the generalized reduced gradient (GRG) method. However, the theorem and mathematical computation procedure in the approach proposed by Chen et al. (1998) are rather complicated. To overcome this problem, Chou and Chen (2008) developed a more convenient method. This approach combines the Brazilian test and a commercial numerical program (e.g., finite difference program, finite element program or boundary element program), and the iterative solution procedure is shown in Fig. 2 and described briefly as follows:

(1) Brazilian tests are performed on two types of specimens: Type N (the central axis normal to the transversely isotropic plane) and Type P (the central axis parallel to the transversely isotropic plane). The strains at the disc center are obtained by Eq. (4), and ε_H, ε_{45} and ε_V are measured by 45° strain rosettes in the test. The parameters E and ν are calculated by Eq. (5).

(2) The temporary E', ν' and G' are computed by substituting $\varepsilon_x \pi Dt/P$, $\varepsilon_y \pi Dt/P$, $\gamma_{xy} \pi Dt/P$ and SCFs into Eq. (2).

(3) The five elastic constants obtained by the previous steps are applied in the numerical simulation of the Brazilian tests, and the software of Fast Lagrangian Analysis of Continua (FLAC3D) is adopted in this study. The new SCFs are computed by Eq. (1).

(4) Steps (2) and (3) are repeated until E', ν' and G' have converged, and the difference between two successive cycles below 0.1% is adopted as the termination criterion.

$$\begin{Bmatrix} \varepsilon_x \\ \varepsilon_y \\ \gamma_{xy} \end{Bmatrix} = \begin{bmatrix} 1 & 0 & 0 \\ 0 & 0 & 1 \\ -1 & 2 & -1 \end{bmatrix} \begin{Bmatrix} \varepsilon_H \\ \varepsilon_{45} \\ \varepsilon_V \end{Bmatrix} \tag{4}$$

$$\begin{aligned} E &= \frac{16P}{\pi Dt(3\varepsilon_y + \varepsilon_x)} \\ \nu &= -\frac{3\varepsilon_x + \varepsilon_y}{3\varepsilon_y + \varepsilon_x} \end{aligned} \tag{5}$$

Meanwhile, to determine the elastic constants for a transversely isotropic medium, E, ν, E', ν' and G' must satisfy the following thermodynamic constraints (Amadei 1996; Chen et al. 1998):

$$\begin{aligned} &E,\ E',\ G' > 0 \\ &-1 < \nu < 1 \\ &1 - \nu - 2\frac{E}{E'}(\nu')^2 > 0 \end{aligned} \tag{6}$$

2.3 Typical tensile failure criteria for transversely isotropic rocks

Regarding the variation in the tensile strength of transversely isotropic rocks with loading direction, Hobbs (1967) proposed the first failure criterion based on the Griffith crack theory. Afterwards, an anisotropic tensile strength criterion was proposed by Barron (1971) using the modified Griffith's theory. In essence, the two criteria are consistent and combined together as the Hobbs-Barron (H-B) criterion (Ma et al. 2017). Subsequently, Nova and Zaninetti

(1990) presented a continuous tensile strength criterion, called the Nova-Zaninetti (N-Z) criterion, which reproduced the variation in the direct tensile strength of the Luserna gneiss with reasonably good accuracy. Recently, another tensile failure criterion was proposed by Lee and Pietruszczak (2015) employing the single plane of weakness (SPW) theory, so the criterion is called the SPW criterion. Meanwhile, based on the tensile strength tensor, Lee and Pietruszczak (2015) also proposed another tensile failure criterion, named the Lee-Pietruszczak (L-P) criterion, which tends to oversimplify the real tensile strength features. These criteria are expressed in detail as follows:

(1) H-B Criterion (Barron 1971; Hobbs 1967):

$$T(\beta)=\begin{cases}\dfrac{2T_b}{\cos\beta(1+\cos\beta)}, & 0^\circ\le\beta\le\beta^*\\ T_m, & \beta^*\le\beta\le 90^\circ\end{cases} \tag{7}$$

with $\cos\beta^*(1+\cos\beta^*)=\dfrac{2T_b}{T_m}$.

(2) N-Z Criterion (Nova and Zaninetti 1990):

$$T(\beta)=\frac{T_bT_m}{T_b\sin^2\beta+T_m\cos^2\beta} \tag{8}$$

(3) SPW Criterion (Lee and Pietruszczak 2015):

$$T(\beta)=\begin{cases}\dfrac{T_b}{\cos^2\beta}, & 0^\circ\le\beta\le\beta^*\\ T_m, & \beta^*\le\beta\le 90^\circ\end{cases} \tag{9}$$

with $\beta^*=\cos^{-1}\sqrt{\dfrac{T_b}{T_m}}$.

(4) L-P Criterion (Lee and Pietruszczak 2015):

$$T(\beta) = \frac{T_m + T_b}{2} - \frac{T_m - T_b}{2}\cos 2\beta \tag{10}$$

where $T(\beta)$ denotes the tensile strength of a specimen when the angle between the loading direction and the transversely isotropic plane is β; T_m and T_b represent the tensile strengths of the rock matrix and the weak planes (e.g., bedding plane, foliation plane and discontinuity plane), respectively.

2.4 Size-effect models

When the sample shape, e.g., length-to-diameter ratio, is prescribed, the sample diameter can be selected as the size-dependent representative parameter since the variation in the diameter is directly related to the volumetric change in the sample (Masoumi et al. 2018). To our knowledge, although the existing size-effect models reviewed extensively by Masoumi et al. (2015) are all derived from isotropic materials, they are very important references to deduce the size-effect model for transversely isotropic rocks.

Based on the statistical theory, viz., the weakest-link theory, a statistical model was first proposed to describe the relationship between material strength and sample size (Weibull 1951). Furthermore, from the viewpoint of fracture energy, a size-effect law (SEL) was put forward by Bažant (1984), who explained that the size dependency in brittle and quasi-brittle materials, e.g., concrete and rock, was caused by the blunting of microcracking prior to the fracture. Subsequently, size effect studies were carried out by Carpinteri et al. (1995) on Brazilian tensile strength data of concrete specimens, and a multifractal scaling law (MFSL) was proposed. In addition, the concept of fractals was introduced into fracture energy by Bažant (1997), who presented a fractal fracture size-effect law (FFSEL). The former three

size-effect models are the descending type, but the last one is the only ascending type. All four size-effect models are given in the following:

(1) Statistical Model (Weibull 1951):

$$\frac{\sigma_t}{\sigma_{t50}} = (\frac{50}{d})^k \tag{11}$$

(2) SEL (Bažant 1984):

$$\sigma_t = \frac{Bf_t}{\sqrt{1+\frac{d}{\lambda d_0}}} \tag{12}$$

(3) MFSL (Carpinteri et al. 1995):

$$\sigma_t = f_c\sqrt{1+\frac{l}{d}} \tag{13}$$

(4) FFSEL (Bažant 1997):

$$\sigma_t = \frac{\sigma_0 d^{\frac{d_f-1}{2}}}{\sqrt{1+\frac{d}{\lambda d_0}}} \tag{14}$$

where σ_t is the tensile strength; d is the sample diameter; k is a positive constant; σ_{t50} denotes the tensile strength obtained from a specimen of 50 mm diameter; B and λ are dimensionless material constants; f_t represents the strength of a specimen with an infinitesimal size; d_0 represents the maximum aggregate size; f_c denotes the strength of a specimen with an infinite size; l is a material constant with unit of length; σ_0 has the same meaning as f_t; and d_f denotes the fractal dimension.

3. Materials and methods

3.1 Sample preparation

To minimize the influence of discreteness, five blocks of slate were taken from the same location in a slate quarry in Jiujiang, Jiangxi Province, China. The slate is a metamorphic Precambrian rock from sedimentary rocks. The slate, which exhibits dark gray to light gray colors, possesses a well-developed slaty structure with very straight layers (Fig. 3a), compared to the rippled layers of shale. Moreover, a thin section of the slate normal to the foliation planes is observed by optical microscopy and shown in Fig. 3b. The sample has a layered texture composed of granular calcite (5%), flaky sericite (25-30%) and angular feldspar and quartz (65-70%) with a very fine grain size in the range of 0.01-0.05 mm. Fig. 3c further shows using SEM that the slate is tightly packed with strongly oriented rock fragments. The natural density of the slate is 2759 ± 5 kg/m^3.

The core specimens were drilled parallel to the foliations (Type P) and perpendicular to the foliations (Type N) with diameters of 25, 38, 50, 63, 75 and 100 mm and were then cut into disc specimens. The thickness (t) of each disc specimen was fixed at 0.5 times the diameter (D) of the specimen. The end surfaces of the disc specimens were polished to satisfy the standard for the tests (ASTM 2016). The P-wave velocities of the slate samples were tested with inclination angles (β) of 0°, 15°, 30°, 45°, 60°, 75° and 90° by using a Tektronix DPO 2012B oscilloscope, OLYMPUS 5077PR wave pulser/receiver and two OLYMPUS V195 ultrasound probes. The variation in the P-wave velocities (v_p) with β is depicted in Fig. 4. The results indicate that the v_p decreases from 6002 to 4760 m/s with increasing β because of the increased influence of foliations on the ultrasound transmission within the slate sample. Based on the anisotropy classification proposed by Tsidzi (1997), using a velocity anisotropy

index (VA) expressed as Eq. (15), the slate (VA=22.9) is classified as a highly anisotropic rock.

$$VA = \frac{V_{\max} - V_{\min}}{V_{mean}} (\%) \tag{15}$$

in which $V_{\max}$, $V_{\min}$ and V_{mean} are the maximum, minimum and average ultrasonic wave velocities, respectively.

3.2 Test procedure

To ensure accuracy, a VJ tech machine with a low loading capacity of 100 kN was employed to conduct the Brazilian tests. The loading rate was controlled at 0.3 mm/min. Among the typical loading configurations suggested by ASTM (2016) and ISRM (1978), the flat loading platens were chosen for this size-effect study. The reason behind this is that the ratio of the steel rod diameter to the specimen diameter (for flat loading platens with two small-diameter steel rods) or the contact angle (for curved loading jaws) is a function of the specimen diameter, which will greatly affect the measured tensile strength (Komurlu and Kesimal 2015; Markides and Kourkoulis 2012; Rocco et al. 1999). In addition, strains at the disc center of the specimen were obtained by a 45° strain rosette with a length of 3 mm, which should not exceed 10% of the diameter of the disc (Chen et al. 1998). During the test, the load and strains were recorded simultaneously using a Kyowa datalogger. The fracture conditions of the specimens in the test were recorded through a Photron FASTCAM SA-Z high-speed camera with LED lighting.

4. Results and discussion

4.1 Size effect on the elastic properties

Fig. 5a and b show the typical stress-strain curves of the disk-shaped slate samples of Type N and Type P, respectively. The $\varepsilon_x \pi Dt/P$, $\varepsilon_y \pi Dt/P$ and $\gamma_{xy} \pi Dt/P$ used in section 2.2 to compute E', ν' and G' correspond to the secant values at 50% peak stress as depicted by the green lines in Fig. 5.

Theoretically, only two disk-shaped samples are needed to determine the five elastic constants of transversely isotropic rocks by the Brazilian tests. To ensure accuracy, in this study, more than two specimens were employed to measure the elastic constants of the slate for each size, as listed in Table 1. The E, E', G', ν and ν' results for each size slate specimen are listed in Table 1 and plotted in Fig. 6. Parameter E dramatically increases as the sample diameter increases from 25 to 38 mm, then fluctuates when the sample diameter is in the range of 38-75 mm, and finally increases again until the sample diameter reaches 100 mm. The total trend of E increases with specimen size, which is similar to that observed in the Blanco Mera granite (Quiñones et al. 2017) and Stanstead granite (Walton 2017). This is because E and ν are obtained by Type N samples, in which the foliation planes have little influence on the deformability of transversely rocks under the Brazilian tests. At this point, the slate of Type N and the two granites are treated as isotropic rocks, irrespective of rock anisotropy. The ascending size effect on E can be attributed to the near-surface damage during sample preparation. The larger specimens have a lower surface area-to-volume ratio ($8/d$ for the Brazilian discs), so the larger specimens can be expected to be more rigid with less damage densities. In contrast, E', ν' and G' were determined by Type P samples, in which the foliation planes have a great influence on the deformability of transversely isotropic rocks under the Brazilian tests. Moreover, the stiffness of the foliation plane is far

smaller than that for the rock matrix. The increasing number or volume of foliation planes per unit volume in the loading direction with increasing sample diameter reduces the rigidity of the sample, which can explain the decrease with the sample diameter as shown in Fig. 6a for E' and G'. The singularities of E' for the 38-mm-diameter sample and of G' for the 50-mm-diameter sample may be induced by the greater effect of the surface damage in sample preparation than that of the foliation plane. Additionally, ν and ν' do not present an evident size effect, as depicted in Fig. 6b.

The shear modulus G' is often obtained (Togashi et al. 2017) using Saint-Venant's empirical relation (Saint Venant 1863) as follows:

$$\frac{1}{G'_{SV}} = \frac{1}{E} + \frac{1}{E'} + 2\frac{\nu'}{E'} \tag{16}$$

Cho et al. (2012) investigated the validity of the empirical equation and found that the equation did not agree well with the experimental data obtained from Asan gneiss, Boryeong shale and Yeoncheon Schist. With respect to this issue, the results of G' obtained from experiment and theory for the slate of various diameters are compared and shown in Fig. 7. The results demonstrate that with increasing sample diameter, the difference between G' measured by experiment and that predicted by theory decreases gradually, almost equal to zero when D=100 mm.

4.2 Size effect on the tensile strength

As mentioned in the introduction section, the indirect tensile strength (σ_t) is well approximated as the principal tension at the disc center, expressed as follows (Claesson and Bohloli 2002):

$$\sigma_t = \frac{2P}{\pi Dt}\left[(\sqrt[4]{E/E'})^{(-\cos 2\beta)} - \frac{\cos 4\beta}{4}(b-1) \right] \tag{17}$$

where $b = \frac{\sqrt{EE'}}{2}(\frac{1}{G'} - \frac{2\nu'}{E'})$.

For each condition (a prescribed size and β), there are three to five slate samples being tested. The tensile strength results for each of the samples tested are plotted in Fig. 8. The results indicate that the variation in σ_t with β for specimens of different sizes mostly exhibits trend III: σ_t increasing systematically with β. Sometimes the minimum σ_t occurs at 15° or 30°, which is consistent with the results observed in other transversely isotropic rocks (Khanlari et al. 2015; Mighani et al. 2016).

4.2.1 Assessment of tensile failure criteria

To assess the performance of existing typical tensile failure criteria, as mentioned in section 2.3, three different assessment indicators are employed. They are the maximum absolute relative error (*MARE*), the average absolute relative error (*AARE*), and the standard error (*SE*), defined by the following formulae:

$$MARE = \max\left\{ \left| \frac{T_P(\beta) - T_E(\beta)}{T_E(\beta)} \right| \right\} \tag{18}$$

$$AARE = \frac{\sum \left| \frac{T_P(\beta) - T_E(\beta)}{T_E(\beta)} \right|}{N} \tag{19}$$

$$SE = \sqrt{\frac{\sum [T_P(\beta) - T_E(\beta)]^2}{N}} \tag{20}$$

The three assessment indicators can reflect the reliability or misfit of each failure criterion, and the higher *MARE*, *AARE* and *SE* indicate the lower reliability and higher misfit, and vice versa. The order of the failure criteria is sorted according to the magnitude of the *MARE*, *AARE* and *SE* when the four failure criteria are evaluated. Note that the *SE* is recommended as the final assessment indicator if the order of the *MARE*, *AARE* and *SE* is not the same for a certain failure criterion (Ma et al. 2017).

The comparisons between the predicted and test results are shown in Fig. 8, and the evaluation results using the *MARE*, *AARE* and *SE* are listed in Table 2. The results indicate that the orders of the reliability of the failure criteria are as follows: (1) N-Z > L-P > H-B > SPW for the 25-, 38- and 50-mm-diameter specimens, (2) N-Z > H-B > L-P > SPW for the 63- and 100-mm-diameter specimens, and (3) L-P > SPW > N-Z > H-B for the 75-mm-diameter specimens. Except for the 75-mm-diameter specimens, the predicted results by the N-Z criterion are the most in line with those from the experiments. Therefore, the N-Z criterion is recommended to describe the anisotropy of the tensile strength of the slate.

4.2.2 Anisotropic size-effect of the tensile strength

Based on the existing size-effect models referred to in section 2.4 and the experimental data of this study as shown in Fig. 9, three principles defining the size-effect response are as follows:

(1) The relationship between the tensile strength and specimen size depends on the mechanical properties of the material.
(2) The variation in the tensile strength with specimen size shows both ascending and descending trends and is correlated with the loading-foliation angle.
(3) For samples of a prescribed shape, the tensile strength has upper and lower boundaries with varying sample sizes.

Thus, the SEL and FFSEL are recommended to describe the size dependency of the tensile strength of the slate. This combination has the advantages of capturing increasing and decreasing trends with the common parameters (λd_0).

Based on the SEL, when the upper and lower boundaries are considered, the size-effect relation is transformed as follows:

$$T_1(d) = \sigma_M + \frac{(\sigma_0 - \sigma_M)}{\sqrt{1 + \frac{d}{\eta}}} \tag{21}$$

where $T_1(d)$ is the tensile strength of the specimen with a diameter of d ; η=λd_0 is the unit of length; and σ_0 and σ_M are the tensile strengths when $d \to 0$ and $d \to \infty$, respectively.

Correspondingly, the FFSEL is transformed as follows:

$$T_2(d) = \frac{\bar{\sigma}_0 d^{\frac{d_f - 1}{2}}}{\sqrt{1 + \frac{d}{\eta}}} \tag{22}$$

where $T_2(d)$ has the same meaning as $T_1(d)$; d_f represents the fractal dimension; and $\bar{\sigma}_0$ is the tensile strength when $d \to 0$.

The curve-fitted results of Eqs. (21) and (22) are shown in Fig. 9, and the fitting parameters (σ_0, σ_M, η, $\bar{\sigma}_0$ and d_f) of the equations in every loading-foliation direction are listed in Table 3. The fitted curves are in agreement with the experimental data and the correlation coefficients of Eqs. (21) and (22) are greater than 0.73. The results indicate that with increasing specimen diameter, the tensile strength continues decreasing when β ranges from 0° -45°, and the tensile strength increases first and then decreases when β is in the range of 60°-

90° or the specimen belongs to Type N. The transition occurs when β ranges from 45°-60°, which may be attributed to the change in the failure modes in this range. The results are elaborated in the following. When β ranges from 0°-45°, the tensile strength of slate is mainly dependent on the strength of the foliation planes, displaying the failure mostly along the foliation plane. When β ranges from 60°-90° or the specimen belongs to Type N, the tensile strength of the slate is primarily determined by the strength of the rock matrix, exhibiting the failure mostly across the rock matrix. The typical descending size effect can be attributed to Fairhust's theory (Fairhurst 1971), originating from elastic energy principles, that the product of the length of the critical flaw and the square of the strength of the tested sample is constant. The length of the critical flaw is proportional to the specimen size. Accordingly, the strength decreases with increasing specimen diameter. On the other hand, the reverse size effect observed in the slate specimens can be explained by the smaller specimens having lower strength because of the higher surface damage density or the developing cracks inclining more to intersect the free sample surface in the smaller specimens (Quiñones et al. 2017).

Referring to Table 3, σ_0 and σ_M exhibit an almost increasing trend with β; $\bar{\sigma}_0$ also continues increasing as β increases from 60° to 90°; however, the parameters η and d_f are basically constant. It is worth noting that the curve fitting parameters for the Type N specimen are greatly different from those obtained for the Type P specimens, except for η. The results also suggest that the loading direction plays an important role in the size-effect response.

In addition, to compare the anisotropy of the size effect on the tensile strength of the slate, the derivative of Eq. (21) is deduced as follows:

$$T_1'(d) = -\frac{(\sigma_0 - \sigma_M)}{2\eta(1+\frac{d}{\eta})^{1.5}} \tag{23}$$

where $T_1'(d)$ is the derivative of $T_1(d)$. Values of $T_1'(d)$ are negative since $\sigma_0 - \sigma_M$ and η are positive, as listed in Table 3. The values of $T_1'(d)$ are comparable when β=0-30°, reaching the maximum value. $T_1'(d)$ is the minimum value when β=90°. This implies that the downward size effect on the tensile strength of the slate is strongly increasing with β, reaching the strongest value when β=90°.

4.2.3 Anisotropy of the tensile strength

Darlington et al. (2011) found that the results of specimens 300 mm in diameter, at which asymptotic strength is met, are of crucial importance to large-scale design. Accordingly, the tensile strength of the 300-mm-diameter specimen is recommended as the tensile strength of the representative elementary volume (REV), which is termed T_{REV}. The predicted T_{REV} by Eq. (21) are listed in Table 4, which increases steadily with increasing β. Furthermore, the experimental data fitted by Eq. (8) are plotted in Fig. 10, and the curve fitting parameters T_b and T_m are listed in Table 5. T_b, characterizing the tensile strength of weak planes, decreases gradually, and T_m, characterizing the tensile strength of the rock matrix, increases first and then decreases with increasing specimen size. The variation trends correspond to the two kinds of size-effect responses as depicted in the previous section (see Fig. 9). It further illustrates that the transition of the size-effect trends is closely related to the change in the failure modes.

The curve-fitted results agree well with the experimental data, with correlation coefficients > 0.82 for the various specimen diameters (25-300 mm). In summary, the N-Z criterion is

capable of describing the anisotropy of the tensile strength of the slate irrespective of the sample size.

4.2.4 Universal equations for size-effect and strength anisotropy

A unified size-effect relation capturing the relationship among the tensile strength, sample size and loading direction in transversely isotropic rocks is vital for the correct estimation of the rock strength of a certain specimen size in a given loading direction. As σ_M and σ_0 of Eq. (21) and $\bar{\sigma}_0$ of Eq. (22) can be replaced by Eq. (8), two universal equations describing both the size effect and anisotropy in transversely isotropic rocks are proposed in the following forms:

(1) Using Eq. (8) to substitute σ_M and σ_0 of Eq. (21),

$$T_1(d,\beta)=\frac{T_{bM}T_{mM}}{T_{bM}\sin^2\beta+T_{mM}\cos^2\beta}+\frac{\left(\dfrac{T_{b0}T_{m0}}{T_{b0}\sin^2\beta+T_{m0}\cos^2\beta}-\dfrac{T_{bM}T_{mM}}{T_{bM}\sin^2\beta+T_{mM}\cos^2\beta}\right)}{\sqrt{1+\dfrac{d}{\eta}}} \tag{24}$$

where $T_1(d,\beta)$ is the tensile strength of the specimen with a diameter d at a loading-foliation angle β; T_{b0} and T_{m0} are the tensile strength of the weak plane and the rock matrix, respectively, when $d\to 0$; T_{bM} and T_{mM} represent the tensile strength of the weak plane and the rock matrix, respectively, when $d\to\infty$; and η, as mentioned in Eq. (21), denotes a material constant with unit of length (mm).

(2) Using Eq. (8) to substitute $\bar{\sigma}_0$ in Eq. (22),

$$T_2(d,\beta)=\frac{\bar{T}_{b0}\bar{T}_{m0}}{\bar{T}_{b0}\sin^2\beta+\bar{T}_{m0}\cos^2\beta}\bullet\frac{d^{\frac{d_f-1}{2}}}{\sqrt{1+\frac{d}{\eta}}} \tag{25}$$

where $T_2(d,\beta)$ has the same meaning as $T_1(d,\beta)$; $\bar{T}_{b0}$ and $\bar{T}_{m0}$ represent the tensile strength of the weak plane and the rock matrix, respectively, when $d\to 0$; η is the same as that in Eq. (24); and d_f, as mentioned in Eq. (22), is the dimensionless fractal dimension.

If both ascending and descending trends are observed in the experimental data, let $T_1(d_i,\beta)=T_2(d_i,\beta)$, and the specimen diameter (d_i) at which the maximum tensile strength is reached can be determined. According to the experimental data observed in the slate, Eqs. (24) and (25) are fitted as Eqs. (26) and (27) with $R^2 > 0.93$, and the two fitted surfaces are plotted in Fig. 11.

$$T_1(d,\beta)=\frac{1.13\times1.5\times10^{-16}}{1.5\times10^{-16}\sin^2\beta+1.13\cos^2\beta}+\frac{\left(\frac{202.91\times75.61}{75.61\sin^2\beta+202.91\cos^2\beta}-\frac{1.13\times1.5\times10^{-16}}{1.5\times10^{-16}\sin^2\beta+1.13\cos^2\beta}\right)}{\sqrt{1+\frac{d}{0.36}}},\ R^2=0.931. \tag{26}$$

$$T_2(d,\beta)=\frac{12.41\times3.17}{3.17\sin^2\beta+12.41\cos^2\beta}\bullet\frac{d^{\frac{2.61-1}{2}}}{\sqrt{1+\frac{d}{0.36}}},\ R^2=0.968 \tag{27}$$

Combining Eqs. (26) and (27), d_i for β = 60°, 75° and 90° are 41.0 mm, 35.2 mm and 34.1 mm, respectively. The predicted results are comparable to the experimental results (Fig. 9b), presenting a downward trend with increasing β. The corresponding maximum tensile

strengths of the slate for β=60°, 75° and 90° are 13.32 MPa, 18.35 MPa and 21.75 MPa, respectively.

As seen from the discussion, Eqs. (24) and (25) provide a method to obtain the tensile strength of slate with varying sample sizes and anisotropic angles. Moreover, the characteristic properties of the strength of the representative elementary volume, the upward and downward size-effect trends and the specimen diameter corresponding to the maximum strength are all combined to enable a systematic description of the behavior to be assessed. Nevertheless, the two equations suffer from the problem that specimens of different sizes and anisotropic angles are needed to determine the parameters in the equations for a certain material. It is also highlighted that more research into this issue is needed to demonstrate the capability of the proposed equations for other transversely isotropic rocks.

4.3 Size effect on the tensile failure mechanism

4.3.1 Fracture pattern

The failure pattern of a slate specimen under the Brazilian test is nearly two-dimensional, mostly being similar on two flat surfaces. Thus, only the failure pattern on one surface is displayed. Fig. 12 shows the representative fracture patterns of specimens of different sizes at different loading-foliation angles after testing. The sketches of the fracture patterns are also depicted in Fig. 13. The failure pattern is closely related to the loading-foliation angle and specimen size. In total, three types of failure patterns are presented: layer activation failure (type I), mixed failure (type II), and nonlayer activation failure (type III).

As shown in Fig. 13, when β ranges from 0° to 30°, the disc specimen fails mainly in the type I mode; when β ranges from 45° to 60°, the failure pattern of the specimen covers all three types; and when β ranges from 75° to 90°, the failure of the specimen is mostly manifested by

the type III failure mode. This result is consistent with those observed by other researchers (Dan et al. 2013; Tavallali and Vervoort 2010; Tavallali and Vervoort 2013). The Type N specimen fails by single or multiple cracks along the loading direction accompanying the layer activation, as shown in Fig. 13h.

Furthermore, considering the size effect, the percentages of the three failure types of specimens at different loading-foliation angles are listed in Table 6. For β equal to 0° or 90°, the specimen size has little influence on the failure patterns of the specimens. For β varying from 15° to 30°, the failure patterns of the specimens include types I and II, and the percentage of type II increases first and then decreases and then stabilizes with the specimen size. For β increasing from 45° to 60°, the failure patterns of the specimens include all three types, and the percentage of type III increases first and then decreases with increasing specimen size. For β reaching 75°, the failure patterns of the specimens include type II and III, and the percentage of type III increases first and then decreases and then stabilizes with the specimen size.

Generally, the tensile strength of the specimen failed by type III is the highest, that by type II is secondary and that by type I is the lowest. The variation in the failure pattern with the specimen size can account for variation in the tensile strength with the specimen size, as discussed in section 4.2. The percentage of the fracture type is also similar to the relative fracture length used in the previous study (Tavallali and Vervoort 2010; Tavallali and Vervoort 2013).

4.3.2 Transverse strain

The maximum transverse strain is defined as the transverse strain measured by the horizontal strain gage of the strain rosette at failure. As shown in Fig. 14, the specimen size impacts the maximum transverse strains of the slate specimens under diametral loading. The lowest value

of the maximum transverse strain occurs at β = 0° when the specimen diameter is smaller than or equal to 50 mm, while it occurs at β = 15° when the specimen diameter is larger than 50 mm. In general, the maximum transverse strains, regardless of the loading direction, decrease with the specimen diameter, reaching the minimum value at d = 100 mm. Accordingly, based on the maximum extension strain criterion (Li and Wong 2013), the result implies that the slate samples exhibit an increased brittle failure as the specimen size increases, with Type N samples of large size failing by multiple cracks (Fig. 12). This is consistent with the observations in various isotropic rocks, including sandstone, andesite, granite, basalt and monzonite (Bahaaddini et al. 2019; Masoumi et al. 2018; Masoumi et al. 2017; Serati et al. 2017). They stated that the increased brittleness of rocks resulting from the increasing sample size in a Brazilian test would cause the tensile breakage to change from single cracking to multiple cracking, which may undermine the validity of the Brazilian test for brittle rocks. Meanwhile, similar to the size effect on the tensile strength, the size effect on the maximum transverse strain is stronger at high loading-foliation angles than at low loading-foliation angles, reaching the strongest effect at β of 90°.

In addition, it has been found that the contact angle plays an important role in the failure mechanism in the Brazilian test (Bahaaddini et al. 2019). The critical contact angle for the transition from multiple cracking to single cracking is material dependent, which can be estimated by the ratio of the uniaxial compressive strength (UCS) to the tensile strength. As shown in Fig. 15, the UCS to tensile strength ratios of the slate samples do not present an evident size effect but vary with loading-foliation angle. At β of 45° to 90°, the UCS to tensile strength ratios of the slate samples are comparable and in the range of 5 to 10, while at β of 0° to 30°, they range from 15 to 30. According to the recommendation of Bahaaddini et al. (2019), the minimum contact angles required for the slate samples at β of 0° to 30° and 45° to 90° are 14° and 22°, respectively. In this study, the flat loading platen was adopted to

neglect the influence of the contact angle. As an alternative, the curved loading jaw with different radii of curvature regarding samples of different sizes can be used to ensure a constant contact angle (ISRM 1978; Lin et al. 2015). Note that the UCS data of the slate samples are provided in the reference (Li et al., submitted for publication).

It can be concluded that the specimen size, loading-foliation angle and loading configuration together control the failure mechanism of transversely isotropic rocks in the Brazilian test. Due to the presence of weak planes, in the Brazilian test, transversely isotropic rocks are mostly not failed by a single tensile crack initiated at the center. Accordingly, considering the influences of the specimen size, loading-foliation angle and loading configuration, a more reliable solution for the tensile strength of transversely isotropic rocks can be derived in future work.

5 Conclusions

Slate, as a transversely isotropic rock, was employed to investigate the size effect and anisotropy on its deformation, tensile strength and failure mechanism. Disk-shaped slate samples of six sizes ranging from 25-100 mm were cored parallel to (Type P) and normal to (Type N) the foliation planes. A series of Brazilian tests were performed on the slate samples at loading-foliation angles of 0-90° at intervals of 15°. The main findings are summarized as follows:

(1) The Young's modulus (E) in the transversely isotropic plane presents an increasing size effect, while the Young's modulus (E') and shear modulus (G') perpendicular to the transversely isotropic plane exhibit a decreasing size effect. The Poisson's ratios parallel to (ν) and normal to (ν') the transversely isotropic plane do not show an evident size effect. Moreover, the difference between G' obtained from the experiment and Saint

Venant's empirical equation decreases with specimen size. The size effects on these elastic properties of slate can be attributed to the combined influence of foliation planes and near-surface damage during sample preparation.

(2) Irrespective of the sample size, the variation in the tensile strength of slate with loading-foliation angle presents an increasing trend, captured well by the N-Z criterion. At loading-foliation angles of 0°-45°, the tensile strength of the slate presents a typical descending size effect. In contrast, at loading-foliation angles of 60°-90°, the tensile strength of the slate presents a first ascending and then descending size effect. The transition of the size-effect trends is closely related to the failure mechanism. A unified size-effect relation including two equations is proposed and validated against the experimental data on slate. This is the first time that the relationship among the tensile strength, specimen size and loading-foliation angle has been comprehensively captured for the transversely isotropic rock.

(3) With increasing specimen size, the fracture pattern of the specimen at the loading-foliation angle of 0° or 90° does not vary, but at other loading-foliation angles, the percentage of the fracture type with a higher strength increases first and then decreases. Regardless of the loading direction, the maximum transverse strain of the slate under the Brazilian test shows a descending size effect. This implies that the slate samples exhibit an increased brittle failure as the specimen size increases, which is consistent with the observations in various isotropic rocks. It is also found that the specimen size, loading-foliation angle and loading configuration together control the failure mechanism of transversely isotropic rocks in the Brazilian test. Taking these influences into account, a more reliable solution for the tensile strength of transversely isotropic rocks should be derived.

Acknowledgements

The authors thank Dr H. Masoumi for his precious suggestions. They would also like to thank Mr R. Leung for his assistance during the experiment. The work in this paper is financially supported by the Hong Kong Polytechnic University (account RUF4), National Natural Science Foundation of China (Grant No. 51778313) and Cooperative Innovation Center of Engineering Construction and Safety in Shandong Blue Economic Zone.

References

Aliabadian Z, Zhao GF, Russell AR (2017) An Analytical Study of Failure of Transversely Isotropic Rock Discs Subjected to Various Diametrical Loading Configurations. Procedia Engineering 191:1194-1202 doi:https://doi.org/10.1016/j.proeng.2017.05.295

Amadei B (1996) Importance of anisotropy when estimating and measuring in situ stresses in rock. International Journal of Rock Mechanics and Mining Sciences & Geomechanics Abstracts 33:293-325 doi:https://doi.org/10.1016/0148-9062(95)00062-3

Amadei B (2012) Rock anisotropy and the theory of stress measurements. vol 2. Springer Science & Business Media,

ASTM (2016) Standard Test Method for Splitting Tensile Strength of Intact Rock Core Specimens. ASTM International, West Conshohocken, PA

Bahaaddini M, Serati M, Masoumi H, Rahimi E (2019) Numerical assessment of rupture mechanisms in Brazilian test of brittle materials. International Journal of Solids and Structures 180-181:1-12 doi:https://doi.org/10.1016/j.ijsolstr.2019.07.004

Barla G, Innaurato N (1973) Indirect tensile testing of anisotropic rocks. Rock mechanics 5:215-230 doi:10.1007/bf01301795

Barron K (1971) Brittle fracture initiation in and ultimate failure of rocks: part II—Anisotropic rocks: theory International Journal of Rock Mechanics and Mining Sciences & Geomechanics Abstracts 8:553-563

Bažant ZP (1984) Size effect in blunt fracture: concrete, rock, metal. Journal of Engineering Mechanics 110:518-535

Bažant ZP (1997) Scaling of quasibrittle fracture: hypotheses of invasive and lacunar fractality, their critique and Weibull connection. International Journal of Fracture 83:41 doi:10.1023/a:1007335506684

Cai M, Kaiser PK (2004) Numerical Simulation Of The Brazilian Test And The Tensile Strength Of Anisotropic Rocks And Rocks With Pre-Existing Cracks. International Journal of Rock Mechanics and Mining Sciences 41:478-483 doi:https://doi.org/10.1016/j.ijrmms.2004.03.086

Carpinteri A, Chiaia B, Ferro G (1995) Size effects on nominal tensile strength of concrete structures: multifractality of material ligaments and dimensional transition from order to disorder. Materials and Structures 28:311 doi:10.1007/bf02473145

Chen C-S, Hsu S (2001) Measurement of indirect tensile strength of anisotropic rocks by the ring test. Rock mechanics and rock engineering 34:293-321

Chen C-S, Pan E, Amadei B (1998) Determination of deformability and tensile strength of anisotropic rock using Brazilian tests. International Journal of Rock Mechanics and Mining Sciences 35:43-61 doi:https://doi.org/10.1016/S0148-9062(97)00329-X

Cho J-W, Kim H, Jeon S, Min K-B (2012) Deformation and strength anisotropy of Asan gneiss, Boryeong shale, and Yeoncheon schist. International Journal of Rock Mechanics and Mining Sciences 50:158-169 doi:https://doi.org/10.1016/j.ijrmms.2011.12.004

Chou YC, Chen CS (2008) Determining elastic constants of transversely isotropic rocks using Brazilian test and iterative procedure. International journal for numerical and analytical methods in geomechanics 32:219-234

Claesson J, Bohloli B (2002) Brazilian test: stress field and tensile strength of anisotropic rocks using an analytical solution. International Journal of Rock Mechanics and Mining Sciences 39:991-1004 doi:https://doi.org/10.1016/S1365-1609(02)00099-0

Dan DQ, Konietzky H, Herbst M (2013) Brazilian tensile strength tests on some anisotropic rocks. International Journal of Rock Mechanics and Mining Sciences 58:1-7 doi:https://doi.org/10.1016/j.ijrmms.2012.08.010

Darlington WJ, Ranjith PG, Choi SK (2011) The Effect of Specimen Size on Strength and Other Properties in Laboratory Testing of Rock and Rock-Like Cementitious Brittle Materials. Rock Mechanics and Rock Engineering 44:513 doi:10.1007/s00603-011-0161-6

Exadaktylos GE, Kaklis KN (2001) Applications of an explicit solution for the transversely isotropic circular disc compressed diametrically. International Journal of Rock Mechanics and Mining Sciences 38:227-243 doi:https://doi.org/10.1016/S1365-1609(00)00072-1

Fairhurst C Fundamental considerations relating to the strength of rock. In: Colloquium on rock fracture, Ruhr University, Bochum, Germany, Veröff. Inst. Bodenmechanik und Felsmechanik (Karlsruhe). 1971. Citeseer, pp 1-56

Fu H, Zhang J, Huang Z, Shi Y, Chen W (2018) A statistical model for predicting the triaxial compressive strength of transversely isotropic rocks subjected to freeze–thaw cycling. Cold Regions Science and Technology 145:237-248 doi:https://doi.org/10.1016/j.coldregions.2017.11.003

Goodman RE (1989) Introduction to rock mechanics. vol 2. Wiley New York,

Hobbs D (1967) Rock tensile strength and its relationship to a number of alternative measures of rock strength. International Journal of Rock Mechanics and Mining Sciences & Geomechanics Abstracts 4:115-127

Hobbs DW (1964) The tensile strength of rocks. International Journal of Rock Mechanics and Mining Sciences & Geomechanics Abstracts 1:385-396 doi:https://doi.org/10.1016/0148-9062(64)90005-1

Hoek E, Brown ET (1980) Underground excavations in rock. Institution of Mining and Metallurgy, Spon Press, Hertford, London

Hu S, Tan Y, Zhou H, Guo W, Hu D, Meng F, Liu Z (2017) Impact of Bedding Planes on Mechanical Properties of Sandstone. Rock Mechanics and Rock Engineering 50:2243-2251 doi:10.1007/s00603-017-1239-6

ISRM (1978) Suggested methods for determining tensile strength of rock materials. International Journal of Rock Mechanics and Mining Sciences & Geomechanics Abstracts 15:99-103 doi:https://doi.org/10.1016/0148-9062(78)90003-7

Khanlari G, Rafiei B, Abdilor Y (2015) An experimental investigation of the Brazilian tensile strength and failure patterns of laminated sandstones. Rock Mechanics and Rock Engineering 48:843-852

Komurlu E, Kesimal A (2015) Evaluation of indirect tensile strength of rocks using different types of jaws. Rock Mechanics and Rock Engineering 48:1723-1730

Kundu J, Mahanta B, Sarkar K, Singh TN (2018) The Effect of Lineation on Anisotropy in Dry and Saturated Himalayan Schistose Rock Under Brazilian Test Conditions. Rock Mechanics and Rock Engineering 51:5-21 doi:10.1007/s00603-017-1300-5

Lee Y-K, Pietruszczak S (2015) Tensile failure criterion for transversely isotropic rocks. International Journal of Rock Mechanics and Mining Sciences 79:205-215 doi:https://doi.org/10.1016/j.ijrmms.2015.08.019

Li D, Wong LNY (2013) The Brazilian Disc Test for Rock Mechanics Applications: Review and New Insights. Rock Mechanics and Rock Engineering 46:269-287 doi:10.1007/s00603-012-0257-7

Li K, Cheng Y, Fan X (2018) Roles of model size and particle size distribution on macro-mechanical properties of Lac du Bonnet granite using flat-joint model. Computers and Geotechnics 103:43-60 doi:https://doi.org/10.1016/j.compgeo.2018.07.007

Li K, Yin Z, Cheng Y, Cao P, Fan X, Meng J (2019) Size effect and anisotropy in a transversely isotropic rock under compressive conditions. International Journal of Rock Mechanics and Mining Sciences (submitted for publication).

Liao JJ, Yang M-T, Hsieh H-Y (1997) Direct tensile behavior of a transversely isotropic rock. International Journal of Rock Mechanics and Mining Sciences 34:837-849 doi:https://doi.org/10.1016/S1365-1609(96)00065-4

Lin H, Xiong W, Yan Q (2015) Three-dimensional effect of tensile strength in the standard Brazilian test considering contact length. Geotechnical Testing Journal 39:137-143

Loureiro-Pinto J Determination of the elastic constants of anisotropic bodies by diametral compression tests. In: 4th ISRM Congress, 1979. International Society for Rock Mechanics

Ma T, Peng N, Zhu Z, Zhang Q, Yang C, Zhao J (2018) Brazilian Tensile Strength of Anisotropic Rocks: Review and New Insights. Energies 11:304

Ma T, Zhang QB, Chen P, Yang C, Zhao J (2017) Fracture pressure model for inclined wells in layered formations with anisotropic rock strengths. Journal of Petroleum Science and Engineering 149:393-408 doi:https://doi.org/10.1016/j.petrol.2016.10.050

Markides CF, Kourkoulis SK (2012) The Stress Field in a Standardized Brazilian Disc: The Influence of the Loading Type Acting on the Actual Contact Length. Rock Mechanics and Rock Engineering 45:145-158 doi:10.1007/s00603-011-0201-2

Masoumi H, Roshan H, Hedayat A, Hagan PC (2018) Scale-Size Dependency of Intact Rock under Point-Load and Indirect Tensile Brazilian Testing. International Journal of Geomechanics 18:04018006

Masoumi H, Saydam S, Hagan PC (2015) Unified size-effect law for intact rock. International Journal of Geomechanics 16:04015059

Masoumi H, Serati M, Williams DJ, Alehossein H Size dependency of intact rocks with high brittleness: A potential solution to eliminate secondary fractures in Brazilian test. In: 51st US Rock Mechanics/Geomechanics Symposium, 2017. American Rock Mechanics Association,

Mighani S, Sondergeld CH, Rai CS (2016) Observations of tensile fracturing of anisotropic rocks. SPE Journal 21:1,289-281,301

Nova R, Zaninetti A An investigation into the tensile behaviour of a schistose rock. In: International Journal of Rock Mechanics and Mining Sciences & Geomechanics Abstracts, 1990. vol 4. Elsevier, pp 231-242

Quiñones J, Arzúa J, Alejano LR, García-Bastante F, Mas Ivars D, Walton G (2017) Analysis of size effects on the geomechanical parameters of intact granite samples under unconfined conditions. Acta Geotechnica doi:10.1007/s11440-017-0531-7

Rocco C, Guinea GV, Planas J, Elices M (1999) Size effect and boundary conditions in the Brazilian test: Experimental verification. Materials and Structures 32:210 doi:10.1007/bf02481517

Saint Venant B (1863) Sur la distribution des élasticités autour de chaque point d'un solide ou d'un milieu de contexture quelconque, particulièrement lorsqu'il est amorphe sans être isotrope. Journal de Math Pures et Appliquées 8:257-430

Serati M, Masoumi H, Williams DJ, Alehossein H Modified Brazilian test for indirect measurement of tensile strength of brittle materials. In: 51st US Rock Mechanics/Geomechanics Symposium, 2017. American Rock Mechanics Association,

Sesetty V, Ghassemi A (2018) Effect of rock anisotropy on wellbore stresses and hydraulic fracture propagation. International Journal of Rock Mechanics and Mining Sciences 112:369-384 doi:10.1016/j.ijrmms.2018.09.005

Setiawan NB, Zimmerman RW (2018) Wellbore breakout prediction in transversely isotropic rocks using true-triaxial failure criteria. International Journal of Rock Mechanics and Mining Sciences 112:313-322 doi:10.1016/j.ijrmms.2018.10.033

Shang J, Hencher SR, West LJ (2016) Tensile Strength of Geological Discontinuities Including Incipient Bedding, Rock Joints and Mineral Veins. Rock Mechanics and Rock Engineering 49:4213-4225 doi:10.1007/s00603-016-1041-x

Tavallali A, Vervoort A (2010) Failure of Layered Sandstone under Brazilian Test Conditions: Effect of Micro-Scale Parameters on Macro-Scale Behaviour. Rock Mechanics and Rock Engineering 43:641-653 doi:10.1007/s00603-010-0084-7

Tavallali A, Vervoort A (2013) Behaviour of layered sandstone under Brazilian test conditions: Layer orientation and shape effects. Journal of Rock Mechanics and Geotechnical Engineering 5:366-377 doi:https://doi.org/10.1016/j.jrmge.2013.01.004

Togashi Y, Kikumoto M, Tani K (2017) An Experimental Method to Determine the Elastic Properties of Transversely Isotropic Rocks by a Single Triaxial Test. Rock Mechanics and Rock Engineering 50:1-15 doi:10.1007/s00603-016-1095-9

Tsidzi K (1997) Propagation characteristics of ultrasonic waves in foliated rocks. Bulletin of the International Association of Engineering Geology:103-114

Vervoort A et al. (2014) Failure of transversely isotropic rock under Brazilian test conditions. International Journal of Rock Mechanics and Mining Sciences 70:343-352 doi:https://doi.org/10.1016/j.ijrmms.2014.04.006

Walton G (2017) Scale Effects Observed in Compression Testing of Stanstead Granite Including Post-peak Strength and Dilatancy. Geotech Geol Eng doi:10.1007/s10706-017-0377-7

Weibull W (1951) A statistical distribution function of wide applicability. Journal of applied mechanics 18:293-297

Xu G, He C, Chen Z, Wu D (2018) Effects of the micro-structure and micro-parameters on the mechanical behaviour of transversely isotropic rock in Brazilian tests. Acta Geotechnica 13:887-910 doi:10.1007/s11440-018-0636-7

Tables

Table 1 Average values of elastic constants determined on slate samples with different diameters using Brazilian tests.

Diameter of specimen (mm)	No. of tests	E (GPa)	E' (GPa)	ν	ν'	G' (GPa)	E / E'
25	28	56.3	68.1	0.29	0.28	31.2	0.83
38	24	81.4	41.9	0.28	0.30	26.5	1.94
50	25	78.7	55.8	0.28	0.27	30.2	1.41
63	30	71.2	45.2	0.23	0.30	19.4	1.58
75	33	70.1	39.2	0.16	0.20	19.6	1.29
100	29	89.8	28.1	0.32	0.21	16.2	3.19

Table 2 Assessment indicators (*MARE*, *AARE* and *SE*) of slate specimens with different diameters.

Diameter of specimen (mm)	Indicators	Results of the assessment			
		H-B	N-Z	SPW	L-P
25	*MARE*	0.923	0.493	0.923	0.666
	AARE	0.208	0.107	0.258	0.168
	SE	3.801	1.995	4.270	2.832
38	*MARE*	0.454	0.159	0.643	0.369
	AARE	0.117	0.062	0.184	0.167
	SE	2.568	0.863	3.576	2.386
50	*MARE*	0.511	0.381	0.558	0.434
	AARE	0.192	0.166	0.232	0.201
	SE	3.011	2.080	3.888	2.945
63	*MARE*	0.531	0.203	0.770	0.521
	AARE	0.185	0.116	0.261	0.234
	SE	2.199	0.983	3.073	2.271
75	*MARE*	0.322	0.330	0.339	0.186
	AARE	0.147	0.119	0.120	0.090
	SE	1.593	1.420	1.362	0.868
100	*MARE*	0.206	0.195	0.393	0.323
	AARE	0.091	0.089	0.129	0.140
	SE	0.930	0.818	1.591	1.092

Table 3 Fitting parameters in Eqs. (21) and (22) when the slate specimen is loaded in various directions.

β (°)	0	15	30	45	60	75	90	Type N
σ_0 (MPa)	76.45	78.63	77	108.76	127.21	167.16	205.43	153.66
σ_M (MPa)	0	0	0.68	0.95	0.97	1.04	1.13	9.84
σ_0-σ_M (MPa)	76.45	78.63	76.32	107.81	126.24	166.12	204.3	143.82
η					0.36			
R^2	0.73	0.75	0.80	0.81	0.85	0.80	0.83	0.76
$\bar{\sigma}_0$ (MPa)	–	–	–	–	6.75	10.57	12.21	6.54
d_f	–	–	–	–		2.61		2.99
R^2	–	–	–	–	0.79	0.86	0.89	0.88

Table 4 The predicted T_{REV} by Eq. (21) for the slate specimen of d=300mm loaded in various directions.

β (°)	0	15	30	45	60	75	90
T_{REV} (MPa)	2.65	2.72	3.32	4.68	5.34	6.79	8.20

Table 5 The variation in parameters T_b and T_m with specimen size.

Diameter (mm)	25	38	50	63	75	100	300
T_b (MPa)	8.25	7.60	6.32	5.46	5.82	3.80	2.79
T_m (MPa)	18.51	21.58	18.21	16.01	12.55	12.55	8.00
R^2	0.82	0.98	0.88	0.94	0.88	0.97	0.98

Table 6 The percentages of three failure types of slate specimens with different diameters at different loading-foliation angles.

d (mm)	β (°)	Fracture patterns			d (mm)	β (°)	Fracture patterns			d (mm)	β (°)	Fracture patterns		
		% of type I	% of type II	% of type III			% of type I	% of type II	% of type III			% of type I	% of type II	% of type III
	0	100	0	0		0	100	0	0		0	100	0	0
	15	67	33	0		15	0	100	0		15	0	100	0
	30	75	25	0		30	0	100	0		30	50	50	0
25	45	25	25	50	50	45	0	33	67	75	45	0	0	100
	60	50	0	50		60	0	0	100		60	0	25	75
	75	0	25	75		75	0	33	67		75	0	0	100
	90	0	0	100		90	0	0	100		90	0	0	100
	0	100	0	0		0	100	0	0		0	100	0	0
	15	0	100	0		15	25	75	0		15	25	75	0
	30	0	100	0		30	25	75	0		30	50	50	0
38	45	0	0	100	63	45	25	50	25	100	45	0	25	75
	60	0	0	100		60	0	100	0		60	0	25	75
	75	0	0	100		75	0	50	50		75	0	33	67
	90	0	0	100		90	0	0	100		90	0	0	100

Figures

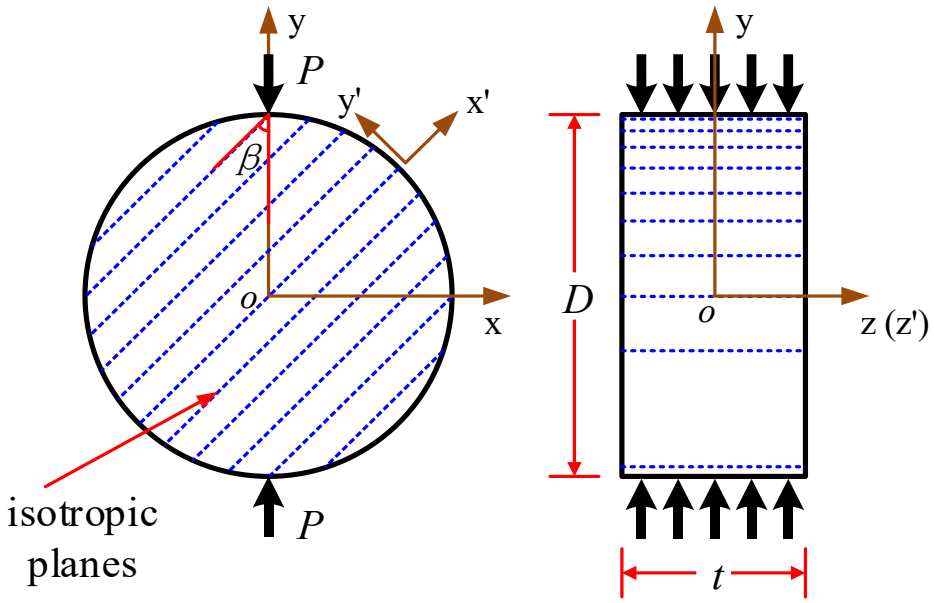

Fig. 1 The disc geometry of a transversely isotropic material under diametral loading.

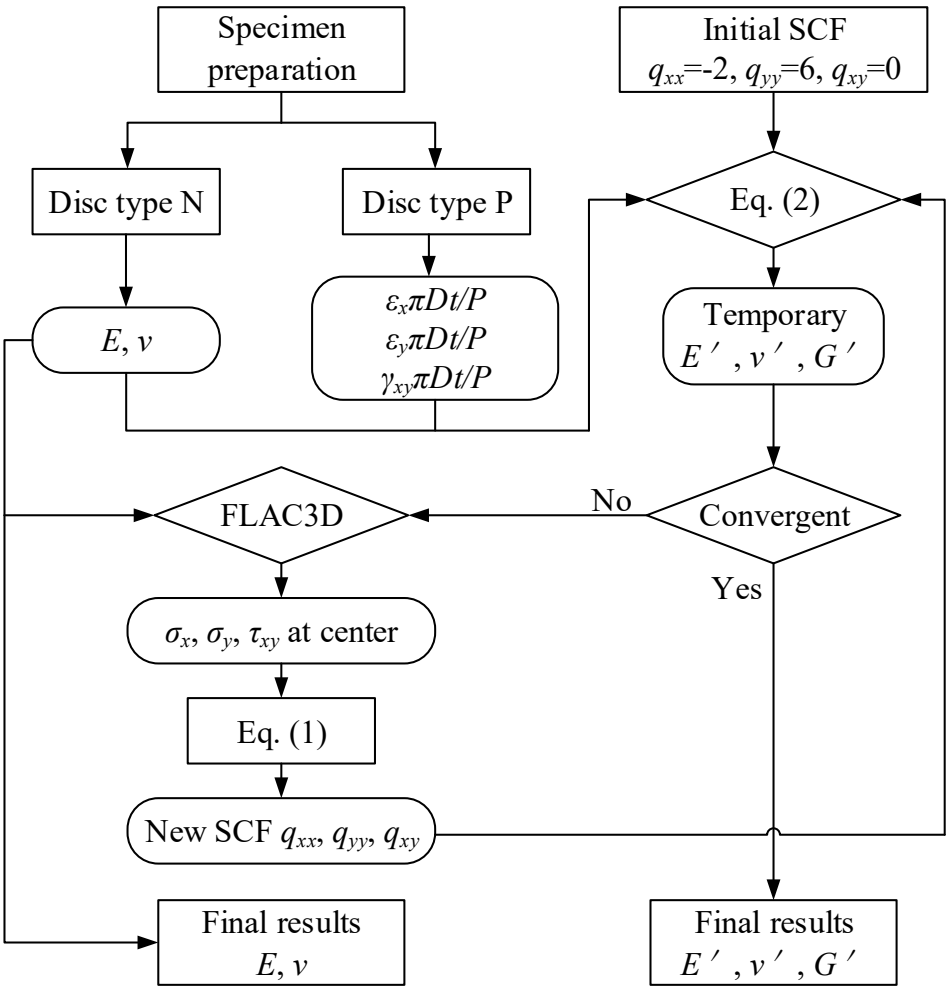

Fig. 2 Flowchart of iteration for calculating the elastic constants modified from Chou and Chen (2008).

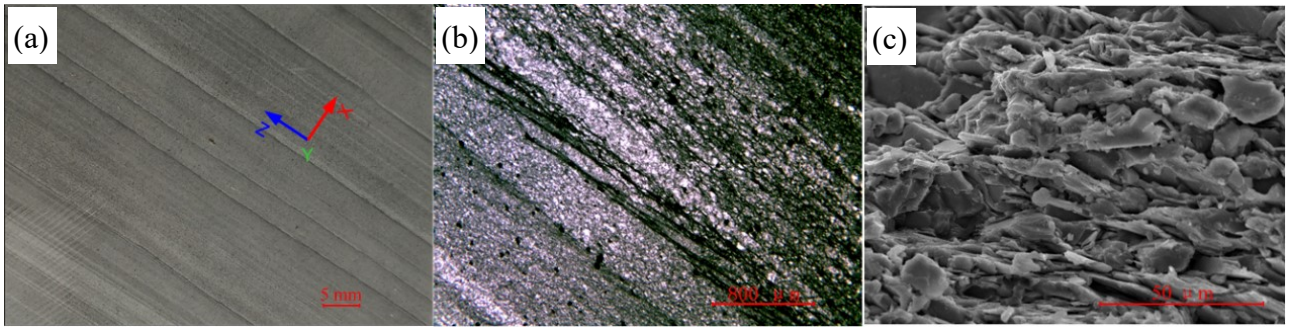

Fig. 3 (a) The appearance of the slate; (b) a thin section image of the slate; (c) a SEM image of the slate.

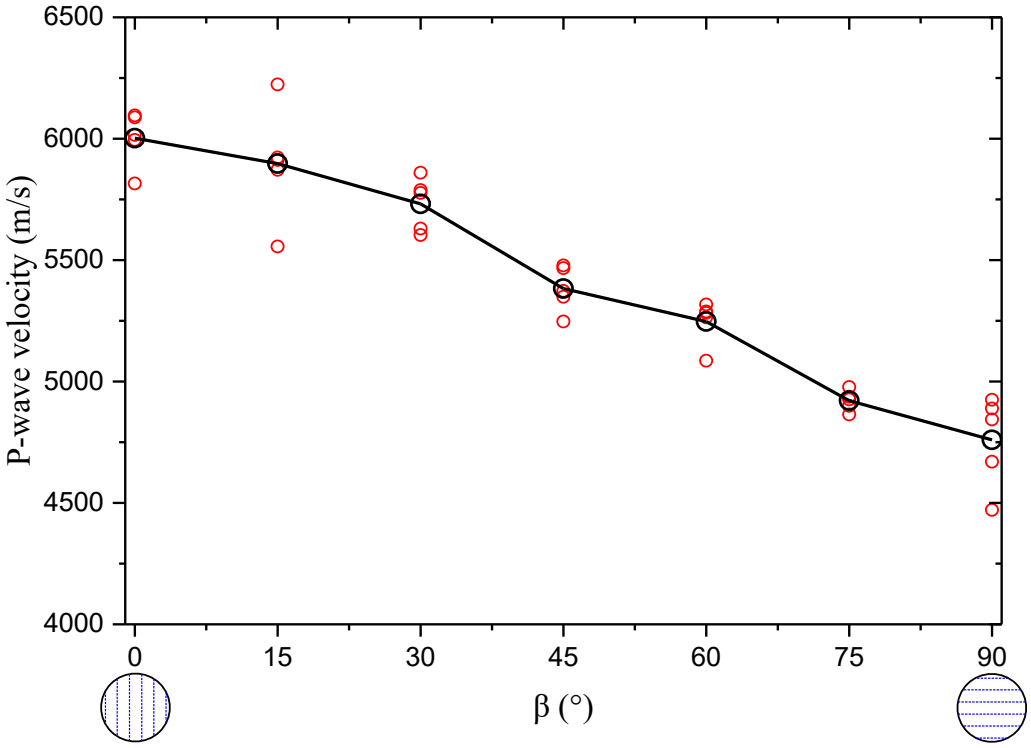

Fig. 4 The variation in P-wave velocities of slate specimens with β. Red circles represent the experimental data and black circles represent the average values.

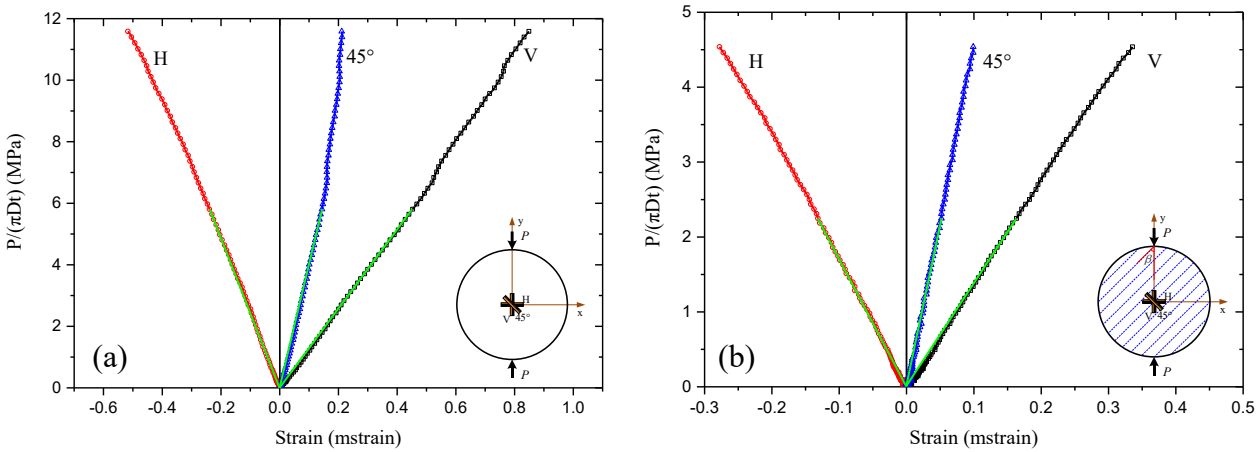

Fig. 5 Typical stress-strain curves of slate specimens under Brazilian tests (strains measured at the centre of the disk): (a) Type N and (b) Type P.

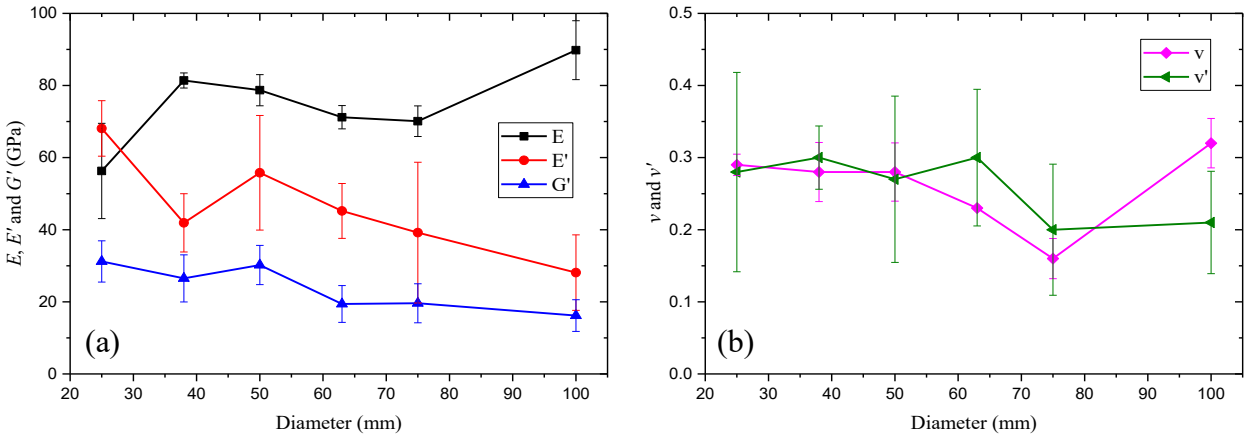

Fig. 6 (a) *E*, *E'*, *G'* and (b) *v*, *v'* results for slate specimens of different diameters. The error bar represents one standard deviation.

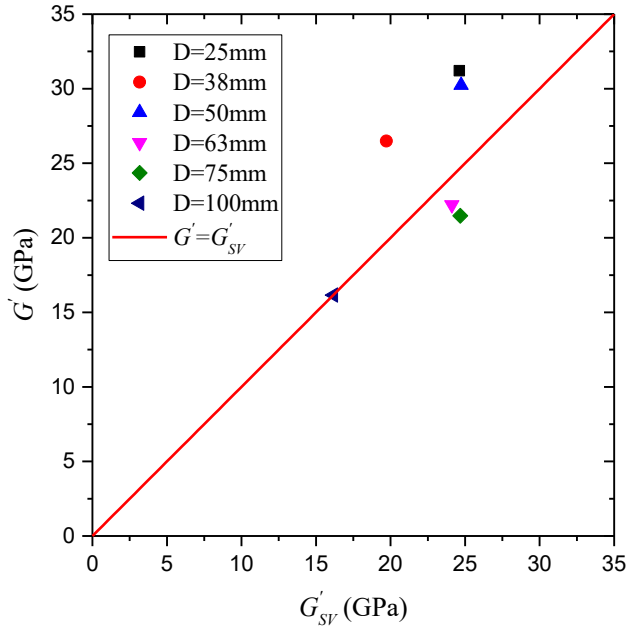

Fig. 7 The comparison between Saint-Venant's empirical values (G'_{SV}) and experimental ones (G').

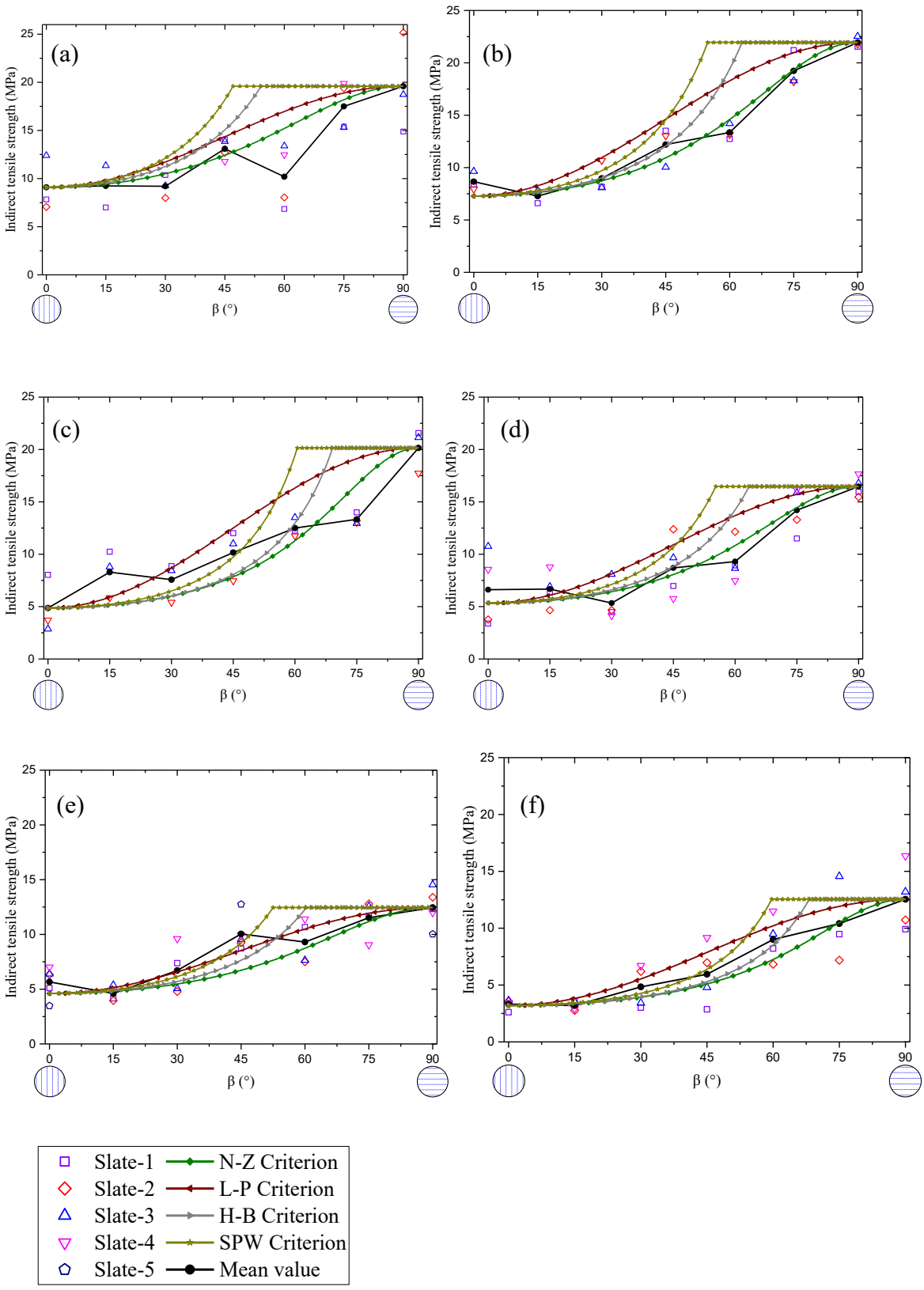

Fig. 8 The relationship between indirect tensile strength and β for slate specimens of different diameters: (a) d=25mm; (b) d=38mm; (c) d=50mm; (d) d=63mm; (e) d=75mm and (f) d=100mm

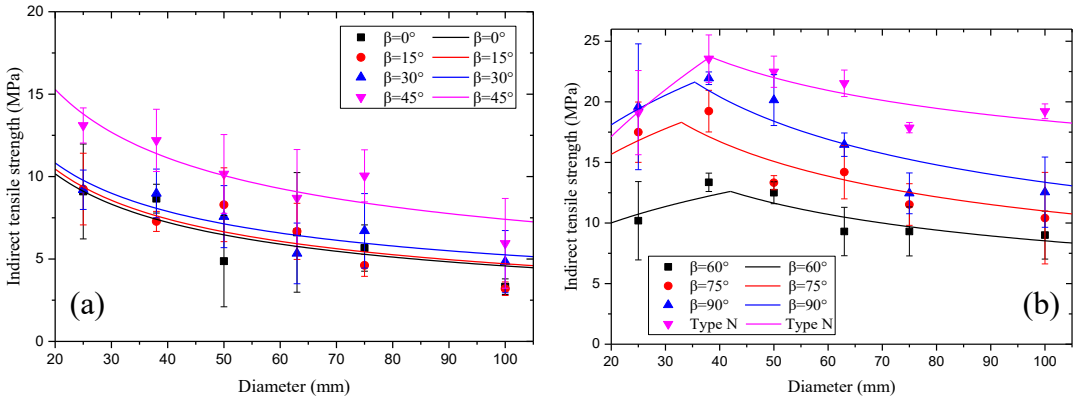

Fig. 9 Size effects on the indirect tensile strength of slate samples at different loading-foliation directions: (a) $\beta = 0° - 45°$; and (b) $\beta = 60° - 90°$ and Type N. The error bar represents one standard deviation.

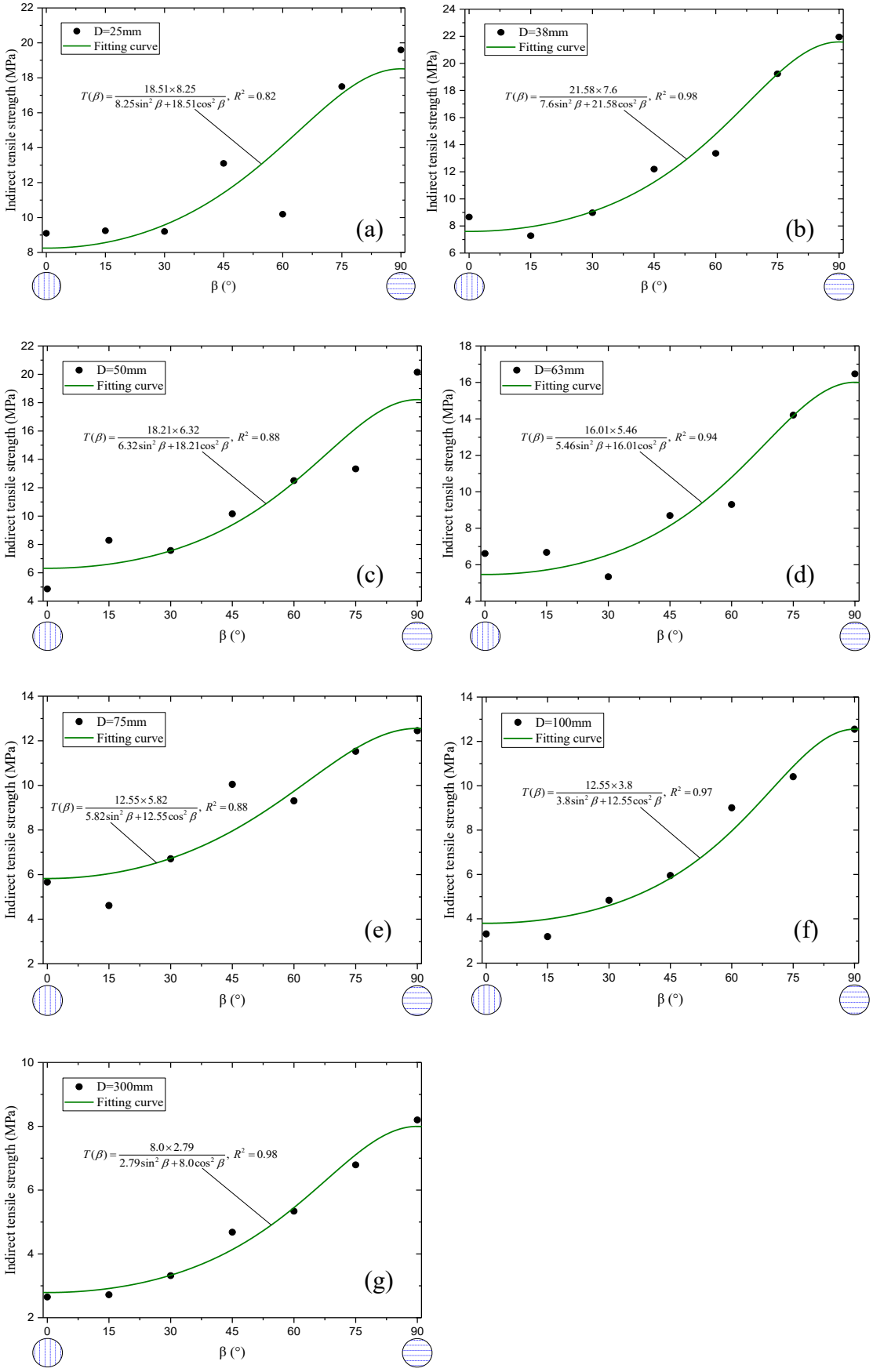

Fig. 10 Comparison of experimental data or predicted T_{REV} with fitted curves by Eq. (8) for slate specimens of (a) *d*=25mm; (b) *d*=38mm; (c) *d*=50mm; (d) *d*=63mm; (e) *d*=75mm; (f) *d*=100mm and (g) *d*=300mm.

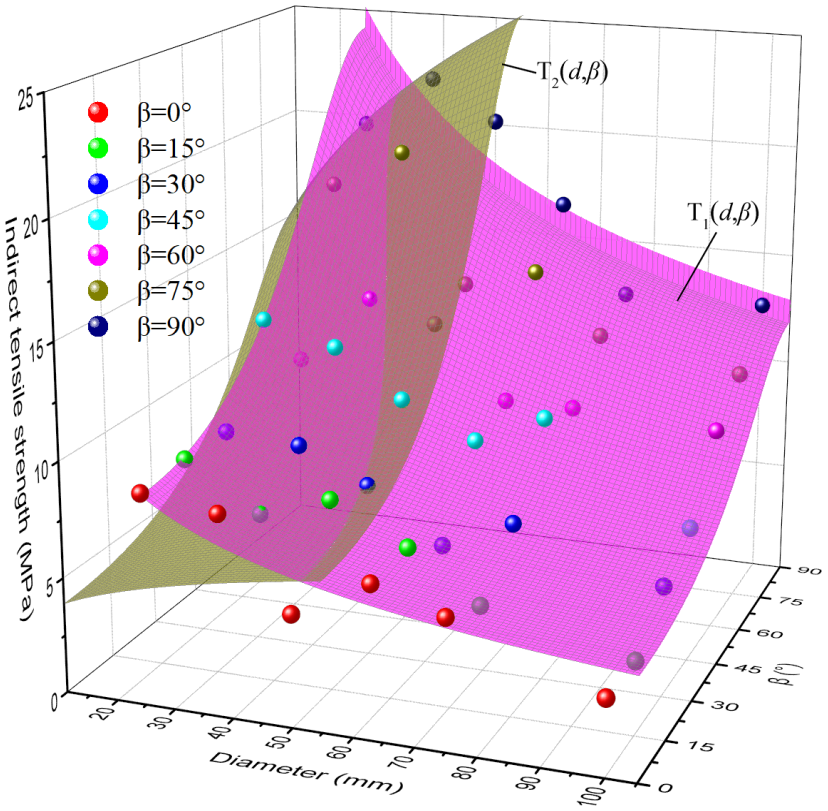

Fig. 11 Comparison of experimental data with two theoretical surfaces fitted by Eqs. (26) and (27) for slate samples of various diameters at different loading-foliation angles.

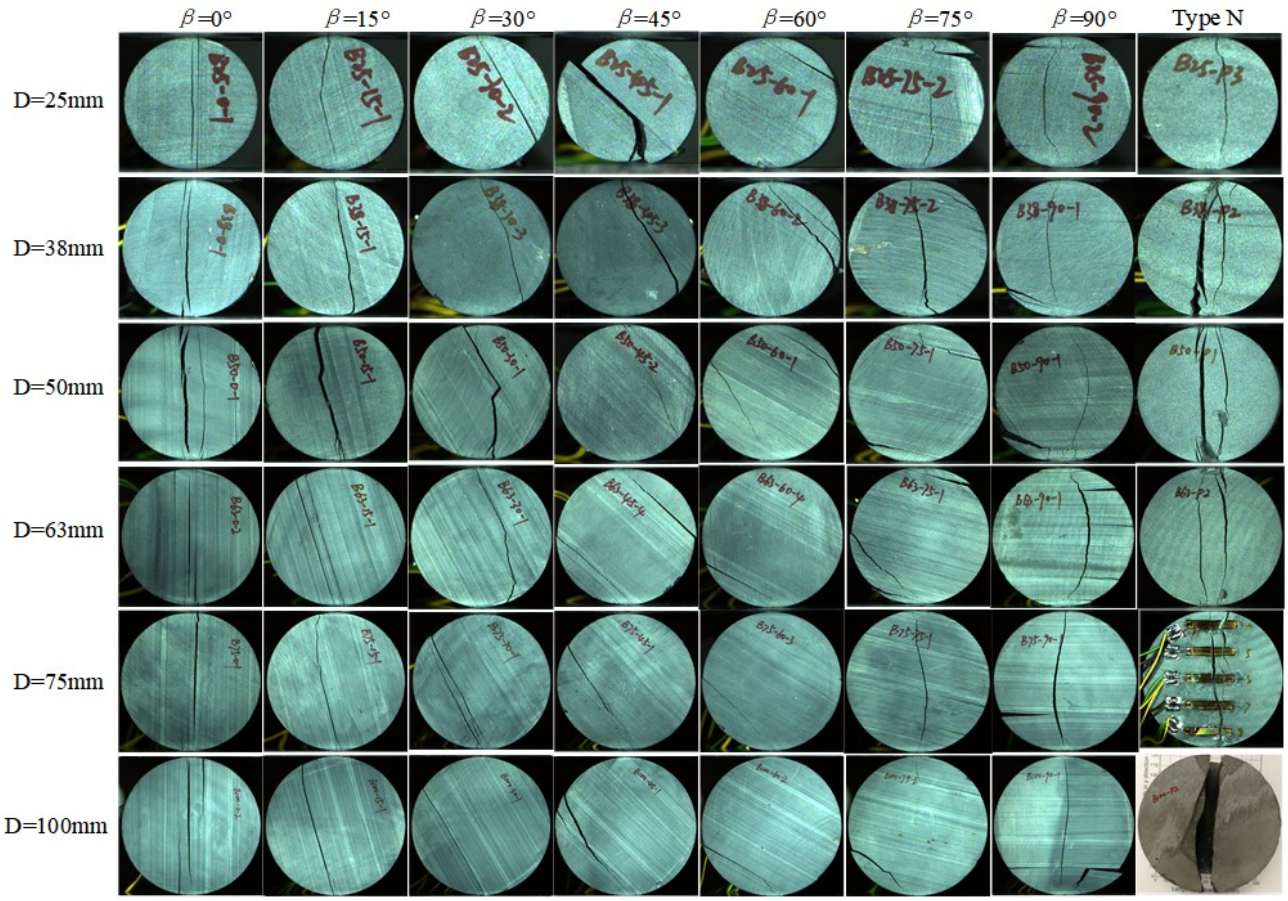

Fig. 12 Representative fracture patterns of slate specimens with different sizes in different loading directions after testing.

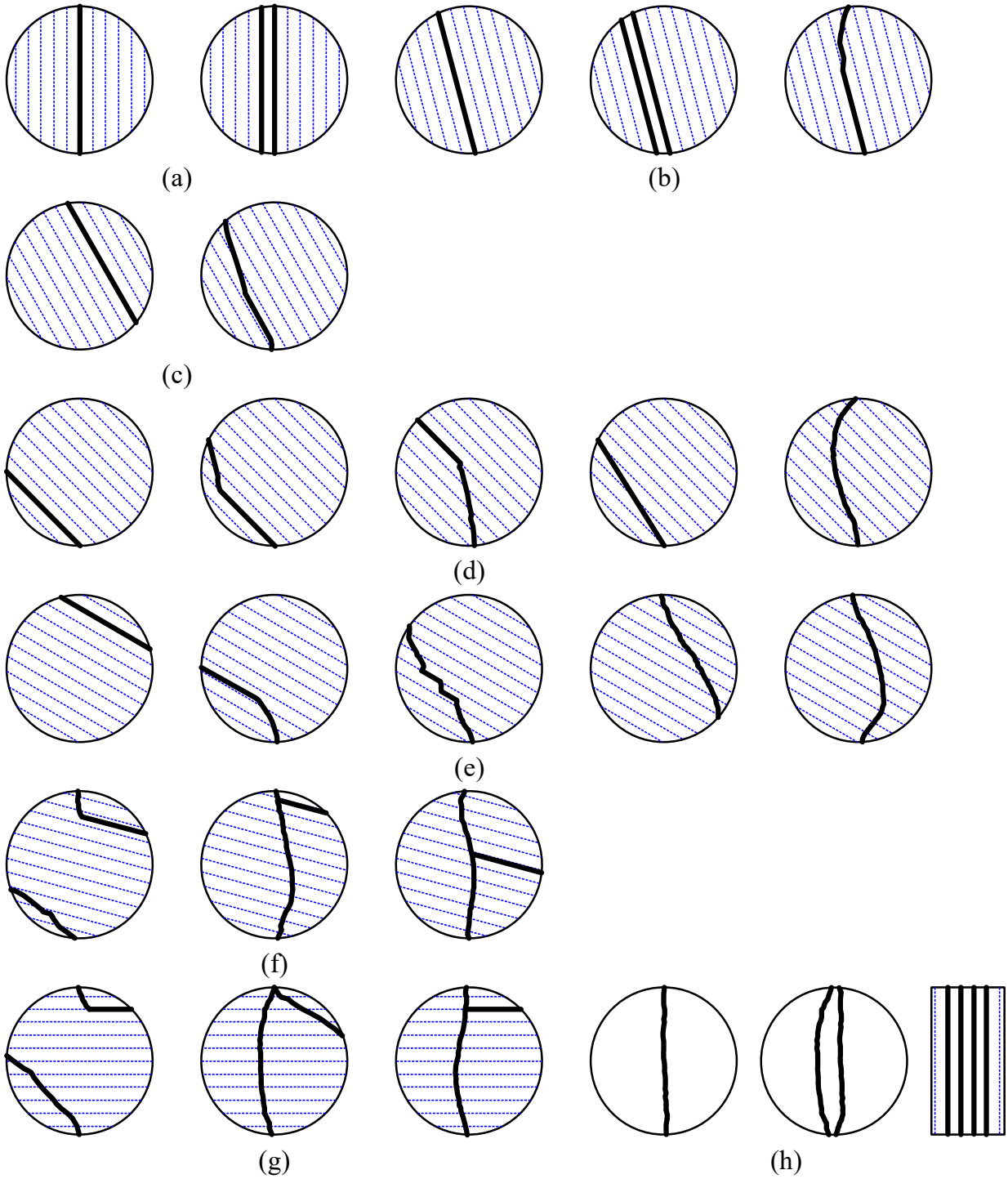

Fig. 13 Sketches of fracture patterns: (a) $\beta = 0°$; (b) $\beta = 15°$; (c) $\beta = 30°$; (d) $\beta = 45°$; (e) $\beta = 60°$; (f) $\beta = 75°$; (g) $\beta = 90°$ and (h) Type N.

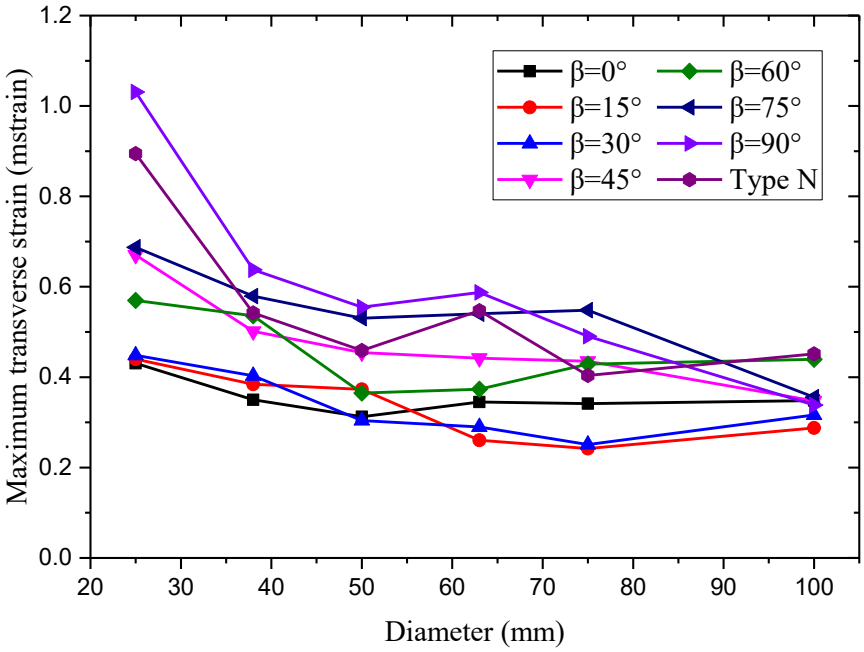

Fig. 14 Size effects on the maximum transverse strains of specimens in different loading directions. The average values are used.

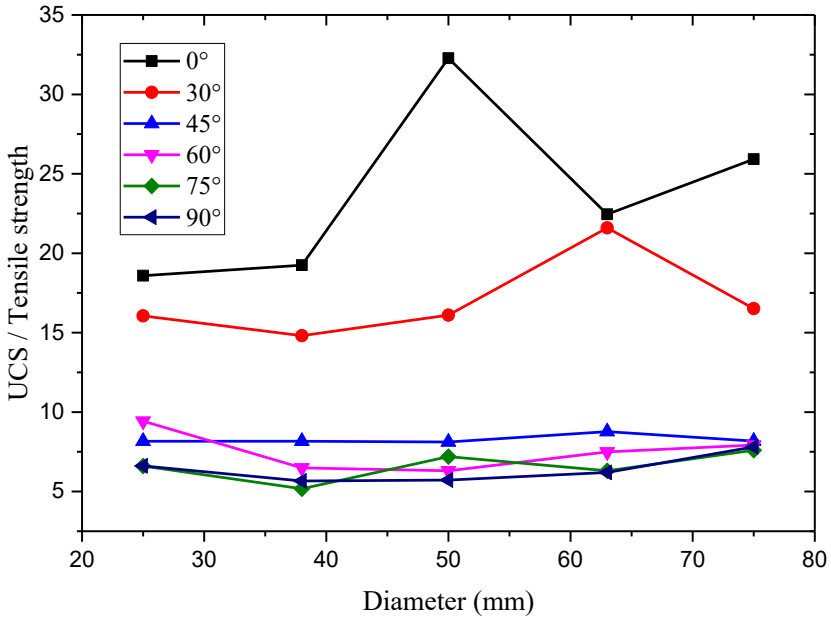

Fig. 15 Size effects on the UCS to tensile strength ratio at different loading-foliation angles. The average values are used.